INTERNATIONAL JOURNAL OF CLIMATOLOGY
Int. J. Climatol. **33**: 1057–1069 (2013)
Published online 11 April 2012 in Wiley Online Library
(wileyonlinelibrary.com) DOI: 10.1002/joc.3489

RMetS
Royal Meteorological Society

Model biases in long coupled runs of NCEP CFS in the context of Indian summer monsoon

Hemantkumar S. Chaudhari,* Samir Pokhrel, Subodh K. Saha, Ashish Dhakate, R. K. Yadav, Kiran Salunke, Somnath Mahapatra, C. T. Sabeerali and Suryachandra A. Rao
Climate and Global Modelling Division, Indian Institute of Tropical Meteorology, Pashan, Pune 411008, India

ABSTRACT: This study examines the performance of National Centers for Environmental Prediction (NCEP) Climate Forecast System (CFS) over the Indian monsoon region in 100 years long coupled run, in terms of biases of sea surface temperature (SST), rainfall and circulation. The study further explores the role of the feedback processes in maintaining these biases. The model simulates reasonable monsoon climatology during JJAS (June–September). It shows dry (wet) rainfall bias concomitant with cold (warm) SST bias over east (west) equatorial Indian Ocean. These biases of SST and rainfall affect both lower- and upper-level circulations in a feedback process, which in turn regulates the SST and rainfall biases by maintaining a coupled feedback process. A dry (wet) rainfall bias over east (west) Indian Ocean induces anomalous low level easterlies over tropical Indian Ocean and causes cold SST bias over east Indian Ocean by triggering evaporation and warm SST bias over west Indian Ocean through advection of warm waters. The persistent SST bias retains the zonal asymmetric heating and meridional temperature gradient resulting in a circum-global subtropical westerly jet core, which in turn magnifies the mid-latitude disturbances and decreases the Mascarene high. The decreased Mascarene high diminishes the strength of monsoon cross-equatorial flow and results in less upwelling as compared to that in the observation. It further increases the SST bias over the West Indian Ocean. The coupled interaction among SST, rainfall and circulation works in tandem through a closed feedback loop to maintain the model biases over tropical Indian Ocean. Copyright © 2012 Royal Meteorological Society

KEY WORDS Climate Forecast System (CFS); model bias; Indian summer monsoon; subtropical westerly jet

Received 5 December 2011; Revised 10 March 2012; Accepted 18 March 2012

1. Introduction

The National Centers for Environmental Prediction (NCEP) Climate Forecast System (CFS) provides operational prediction of the world's climate including the Asian monsoon climate on different time scales. As described by Saha *et al*. (2006), the CFS (Version 1) shows important advances in operational prediction from the previous dynamical forecast efforts by demonstrating a level of prediction skill comparable to statistical methods, at least for the United States. CFS (Version 1) is utilized by various research institutes and universities for seasonal prediction purpose and operational usage. CFS demonstrates skills in simulating El Niño-Southern Oscillation (ENSO) (Wang *et al*., 2005b), the climate over Africa (Thiaw and Mo, 2005), and the sub-seasonal features of the Asian summer monsoon (Yang *et al*. 2008). South Asian summer monsoon variability and intraseasonal variability are investigated by Achuthavarier and Krishnamurthy (2010a, 2010b). Analysis of the retrospective ensemble predictions (hindcasts) of the NCEP CFS indicates that the model successfully simulates many major features of the Asian summer monsoon including the climatology and interannual variability of major precipitation centres and atmospheric circulation systems (e.g. Yang *et al*., 2008; Pattanaik and Kumar, 2010). CFS also depicts the interactive oceanic–atmospheric processes associated with the precipitation anomalies reasonably well at different time leads. Thus, the CFS could be utilized as a better tool for the real-time prediction of Indian summer monsoon rainfall (ISMR).

ISMR contributes about 80% of the annual rainfall over India and thus plays an important role in agriculture, water management and economic planning of this country. The Indian summer monsoon prevails over the Indian region for the four months, from June through September (JJAS). Numerical models have played a vital role in monsoon prediction.

Indian summer monsoon is a deep moist baroclinic system. The following important components of Indian summer monsoon should be reflected in simulation of any numerical model: (1) monsoon trough over central India, (2) low level cross-equatorial flow over west Indian Ocean, (3) upper-level Tibetan high, (4) upper tropospheric tropical easterly jet (TEJ) over peninsular

* Correspondence to: H. S. Chaudhari, Indian Institute of Tropical Meteorology, Pashan, Pune 411008, India.
E-mail: hemantkumar@tropmet.res.in

India, (5) Mascarene high, etc. Several investigators have used atmospheric general circulation models (AGCMs) for simulation of Indian monsoon circulation features and monsoon interannual variability (e.g. Fennessy *et al*., 1994; Sperber and Palmer, 1996; Goswami, 1998; Gadgil and Sajani, 1998; Sabre *et al*., 2000, etc.). However, they noted that simulations were poor for the ISMR. Wang *et al*. (2005a) showed that AGCMs, forced with observed sea surface temperature (SST), are generally unable to simulate the ISMR. They demonstrated that an AGCM coupled with an ocean model simulates realistic SST–rainfall relationships. This suggests that the coupled ocean–atmosphere processes are crucial in the monsoon regions, where atmospheric feedback on SST is critical. Coupled models present a slightly better skill in reproducing the spatial distribution of the rainfall variability (Achuthavarier and Krishnamurthy, 2010b).

Despite the potential for tropical climate predictability, and the advances made in the development of climate models, the seasonal dynamical forecast of Indian summer monsoon remains a challenging problem (e.g. Sperber *et al*., 2001; Sperber and Palmer, 1996; Drbohlav *et al*., 2010; Yang *et al*., 2008; Kang *et al*., 2002; Webster *et al*., 1998; Achuthavarier and Krishnamurthy, 2010b). Substantial efforts are devoted to monsoon prediction by conducting experiments with individual models and approach of multi-model ensembles (e.g. Kang *et al*., 2002; Wang *et al*., 2004; Wu and Kirtman, 2004; Annamalai *et al*., 2005). These efforts involve evaluation of the performance of models in simulating and predicting the monsoon. It is generally believed that skill of monsoon prediction increases when the model features such as atmosphere–ocean–land coupling, resolution and model physics are improved.

Recent studies (Achuthavarier and Krishnamurthy, 2010a, 2010b; Yang *et al*., 2008; Pattanaik and Kumar, 2010) have demonstrated the capabilities of CFS in reproducing mean monsoon distribution and variability. However, none of these studies have tried to explore the model biases and associated feedback processes in maintaining these biases. This study tries to bridge this gap by exploring the seasonal mean monsoon bias over the Indian subcontinent region. The focus of this study is threefold: (1) to find out the model biases in SST, rainfall and circulation features in the long coupled runs of NCEP CFS in simulation of Indian summer monsoon, (2) to explore the possible feedback mechanism among SST, rainfall and circulation in sustaining the model biases and (3) to examine the role of upper-level subtropical westerly jet (SWJ) stream in sustaining model biases and, hence, modulating land–ocean pressure gradient. This paper is organized in the following manner. Brief description of the model including the design of numerical experiments is presented in Section 2. Data and methodology are explained in Section 3. Model biases and its physical interpretation are presented in Section 4. Summary and conclusion are illustrated in Section 5.

2. Model description and design of numerical experiment

The NCEP CFS (Saha *et al*., 2006) is a fully coupled ocean–land–atmosphere dynamical seasonal prediction system composed of the NCEP Global Forecast System (GFS) AGCM (Moorthi *et al*., 2001), and the Geophysical Fluid Dynamics Laboratory (GFDL) Modular Ocean Model version 3 (MOM3) (Pacanowski and Griffies, 1998). The atmospheric component of CFS has a spectral triangular truncation of 62 waves in the horizontal and a finite differencing in the vertical with 64 sigma layers. The model top is at 0.2 hPa. Model physics include solar radiation following Hou *et al*. (1996), the cumulus convection scheme of Hong and Pan (1998), gravity wave drag (Kim and Arakawa, 1995), and cloud water and ice (Zhao and Carr, 1997). The MOM3 uses spherical coordinates in the horizontal and z coordinate in the vertical. The zonal resolution is 1° and the meridional resolution is 1/3° between 10 °S and 10°N and gradually decreases poleward. No flux correction has been implemented in the CFS. The atmospheric and oceanic models are coupled in the region between 65 °S and 50°N while observed and model climatological SST are used to force the model in the region poleward of 65 °S and 50°N. The two components exchange daily averaged quantities, such as heat and momentum fluxes, once per simulated day. The sea ice extent is prescribed from the observed climatology.

The CFS has been ported to an IBM High Performance Computing (HPC) system at IITM (Indian Institute of Tropical Meteorology), Pune. Coupled simulations of CFS are performed by initializing the model on 1 January 1996, and model integration is done for 100 years (model integration period: 1996–2095). The atmospheric initial conditions for the coupled free runs are based on the Reanalysis (R2) data (Kanamitsu *et al*., 2002) and the ocean initial conditions are from the NCEP Global Ocean Data Assimilation System (GODAS). Data from last 30 years of CFS long-term simulation (2066–2095) are considered for the analysis.

3. Data and methodology

To explore model biases, observed data sets such as rainfall from the Climate Prediction Center Merged Analysis of Precipitation (CMAP; Xie and Arkin, 1997); monthly winds, specific humidity, mean sea level pressure (MSLP) from National Centers for Environmental Prediction (NCEP) reanalysis version-2 (Kanamitsu *et al*., 2002); and Reynolds version-2 SST monthly data (Reynolds *et al*., 2002) are utilized in the present study. To explore the dynamical aspect of model biases, moisture transport over the Indian region and surrounding oceanic region is calculated. The vertically integrated water vapour transport $\mathbf{Q}$ is defined as

$$\mathbf{Q} = \frac{1}{g}\int_{P_{300}}^{P_s} q\mathbf{V}dP \qquad (1)$$

where g is the acceleration due to gravity, q the specific humidity, P_s surface pressure, P_{300} the pressure at 300 hPa level up to which moisture is mainly dominant, and **V** is the wind vector (Chen, 1985; Behera *et al*., 1999; Rao *et al*., 2010). Use of the Helmholtz theorem allows us to separate the moisture transport into rotational and irrotational (flux divergence) components.

4. Results and discussions

4.1. Model biases in mean monsoon simulation

4.1.1. Rainfall

Seasonal mean precipitation is characterized by three strong convection zones over the Indian landmass during monsoon season, viz. Central India, the Western Ghats and north-east India. CFS T62 is able to simulate rainfall over the Western Ghats and north-east India; however, it underestimates the rainfall over central India (Figure 1(a) and (b)). It is in agreement with the results of Achuthavarier and Krishnamurthy (2010b). The inability of coupled model to simulate the central Indian rainfall is not unique (Rajeevan and Nanjundiah, 2009). Central Indian rainfall is determined by fluctuation in large-scale circulation patterns in the monsoon trough zone. Monsoon trough coincide with continental tropical convergence zone (CTCZ) during Indian summer monsoon period and most of the transient synoptic scale weather systems form as well as move within this region. CTCZ is an inherent part of the ITCZ (intertropical convergence zone) in the continental region of Indian landmass and it forms as a result of northward migration of ITCZ. It is associated with large-scale convergence, deep convection and precipitation. The rainfall over ITCZ is a result of complex nonlinear interactions among dynamical, thermodynamic, and physical processes. Understanding rainfall over this region is considered as one of the most challenging problems in atmospheric sciences.

The presence of significant dry bias (2–3 mm d^{-1}) over central India implies that CFS underestimates the rainfall over the monsoon trough zone (Figure 1(c)). The time-latitude section of monthly rainfall over core monsoon zone (70°–90 °E) in CFS shows that the high rainfall band migrates up to 22°N (Figure 2(a) and (b)) during the peak monsoon months of July and August. On the other hand, rainfall band migrates up to 27°N in the observation (CMAP). As northward migration of ITCZ is restricted only up to 22 °N in CFS simulations, it could be a probable reason for dry bias over the central Indian region. This argument is further supported by the power spectrum of daily rainfall. It shows that power of 30–60 d mode (which represents northward migration of precipitation) is weaker in CFS as compared to that in the observation (figure not shown). Previous studies have also pointed out that general circulation models are still unable to reproduce the seasonal migration of the ITCZ precipitation (Hack *et al*., 1998; Gates *et al*., 1999; Wu *et al*., 2003).

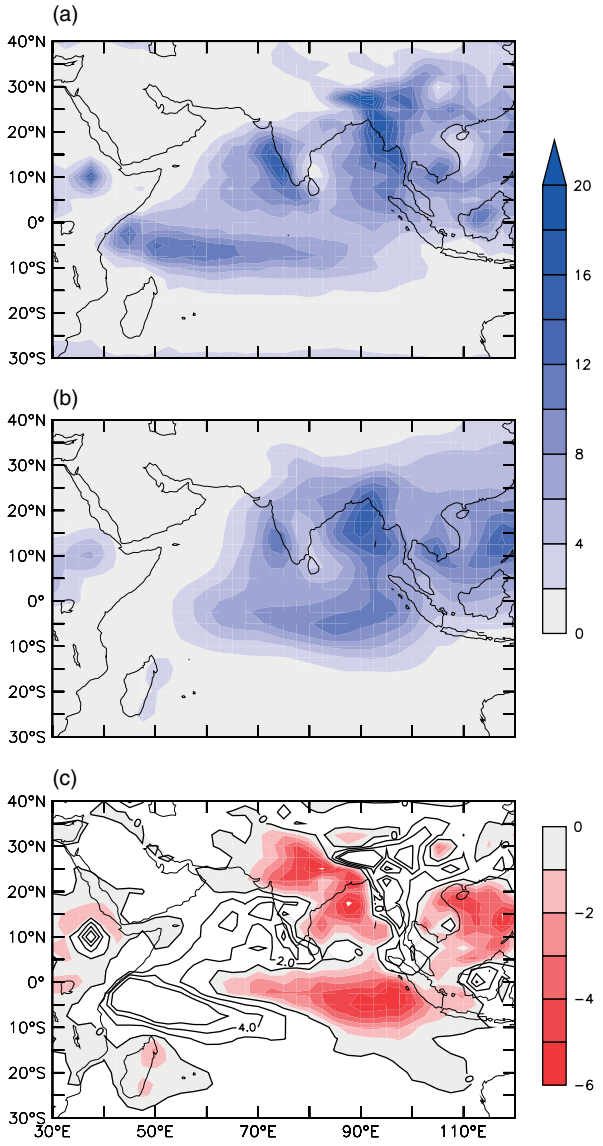

Figure 1. (a) CFS-model-simulated JJAS (June–September) rainfall climatology (mm d^{-1}), (b) CMAP rainfall climatology (mm d^{-1}) for JJAS and (c) model rainfall bias (i.e. difference between CFS and CMAP rainfall, unit: mm d^{-1}). Wet (positive) bias is shown by contours and dry (negative) bias is shown by shaded region.

The oceanic rainfall is a major hindrance in the CFS simulation as it is clear from rainfall bias (Figure 1(c)). The significant wet rainfall bias (2–5 mm d^{-1}) is evident over the western equatorial Indian Ocean (WIO) and Arabian Sea (AS). The presence of dry rainfall bias of similar magnitude over the eastern equatorial Indian Ocean (EIO) and Bay of Bengal (BoB) is also noted. These wet (dry) rainfall biases coincide with the region of warm (cold) SST biases. This is further explained in Section 4.1.2. This indicates that local SSTs might have important role in modulating the rainfall over these regions.

The evolution of rainfall bias over WIO (42°–65 °E; 12 °S–Equator), EIO (82°–100 °E; 9 °S–Equator), AS (50°–70 °E; 4°–20 °N), BoB (averaged over 80°–94 °E; 10°–20 °N) and central Indian region (averaged over

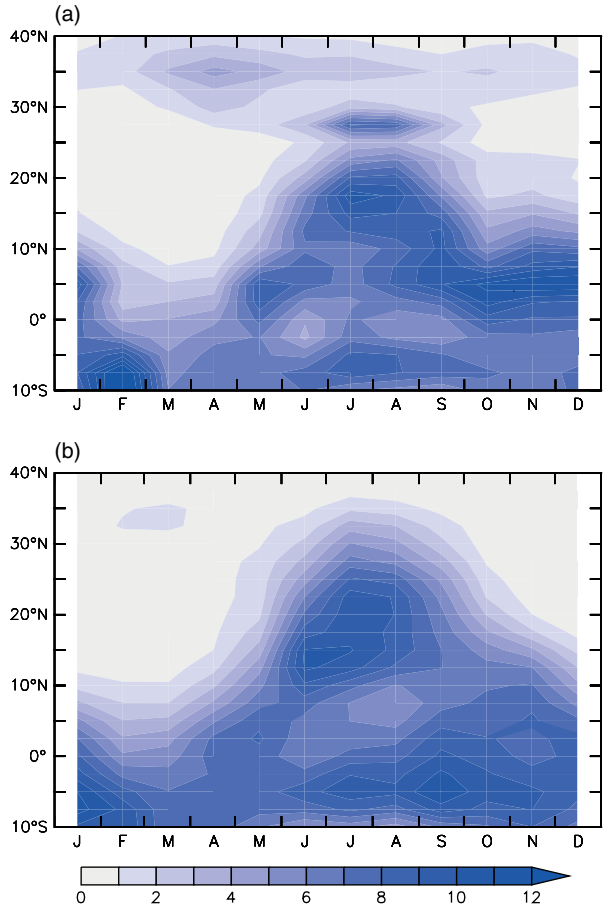

Figure 2. Time-latitude section of (a) CFS T62 rainfall (mm d^{-1}) and (b) climatological CMAP rainfall (mm d^{-1}) averaged over 70 °E–90 °E.

70°–90 °E; 18°–28 °N) is shown in Table I. The seasonal wet rainfall bias over WIO is 5.5 mm d^{-1}; however, dry rainfall bias of 4.4 mm d^{-1} is noted over EIO. It indicates the presence of relatively larger seasonal bias over WIO as compared to that over EIO. Monthly evolutions of rainfall bias indicate that peak monsoon months of July (6.1 mm d^{-1}) and August (5.8 mm d^{-1}) are mainly contributing towards the wet rainfall bias over WIO. However, dry bias is prevailing during the month of September over EIO region. Over the AS wet bias is dominant in the peak monsoon months – July (2.2 mm d^{-1}) and August (2.3 mm d^{-1}). Monthly evolution of rainfall bias is related to different phenomena over different parts of the Indian Ocean basin; in WIO and AS regions, it is owing to the weakening of south westerlies (which generally peak around July and August). In EIO region, local SST–rainfall relationship shows a good correlation (discussed in Section 4.1.3), which may explain some part of this dry rainfall bias.

4.1.2. *Sea surface temperature (SST)*

The Indian Ocean basin has a systematic warm (cold) SST bias over west (east) Indian Ocean (Figure 3) coexisting with model biases in rainfall as discussed in Section 4.1.1. Warm SST bias as large as 2 °C is observed over WIO near Somali coast, which is coinciding with the upwelling region during monsoon season. Cold SST bias of slightly reduced intensity prevails over EIO and covers the areas south of the equator. Warm SST bias spreads over both side of the equator. Cold SST bias over EIO co-occurs with strong easterlies as compared to the observation (Seo *et al*., 2007). These anomalous easterlies induce stronger evaporation and upwelling, leading to the cold SST bias over EIO, and advect warm water to WIO, resulting in warm SST bias. AS

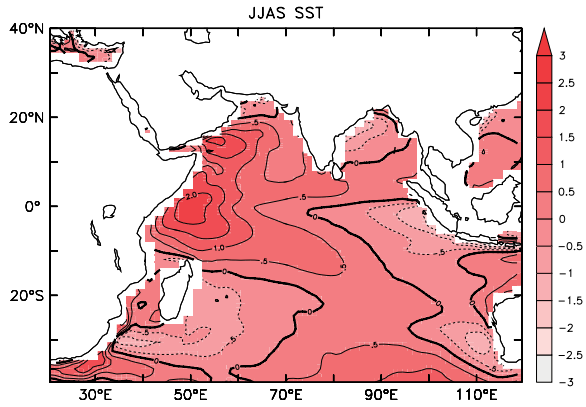

Figure 3. Model SST bias (i.e. difference between CFS-simulated JJAS SST and Reynolds SST in °C). Warm (positive) bias is shown by continuous contours and cold (negative) bias is shown by dotted contours.

Table I. CFS monthly and seasonal rainfall bias (mm d^{-1}) over western equatorial Indian Ocean (WIO: averaged over 42°–65 °E, 12 °S–Equator), eastern equatorial Indian Ocean (EIO: averaged over 82°–100 °E; 9 °S–Equator), Arabian Sea (AS: averaged over 50°–70 °E; 4°–20 °N), Bay of Bengal (BoB: averaged over 80°–94 °E; 10°–20 °N) and central Indian region (averaged over 70°–90 °E; 18°–28 °N).

Month	WIO (42°–65 °E; 12 °S–Equator)	EIO (82°–100 °E; 9 °S–Equator)	AS (50°–70 °E; 4°–20 °N)	BoB (80°–94 °E; 10°–20 °N)	Central India (70°–90 °E; 18°–28 °N)
June	5.5	−2.9	0.1	−3.4	−3.2
July	6.1	−3.7	2.2	−3.9	−2.4
August	5.8	−4.1	2.3	−2.2	−1.5
September	4.5	−6.8	1.8	−0.8	−1.9
June–September	5.5	−4.4	1.6	−2.6	−2.2

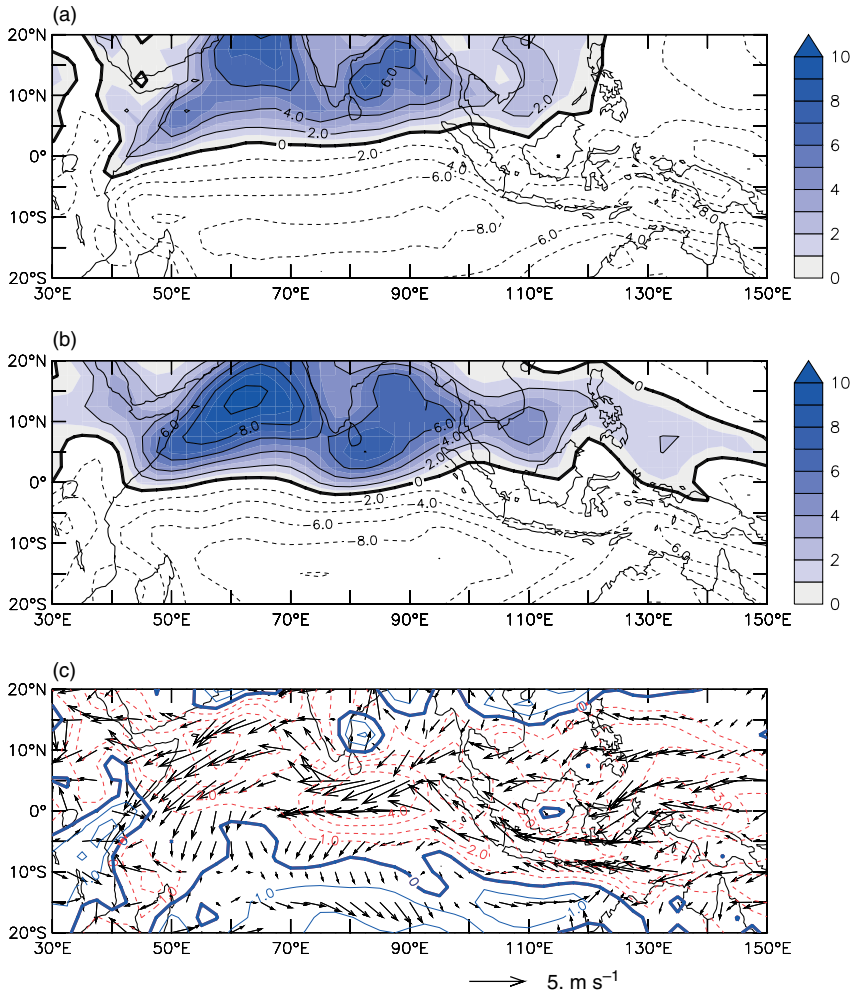

Figure 4. JJAS mean zonal winds (m s^{-1}) at 1000 hPa for (a) CFS and (b) observation (NCEP). Positive zonal wind fields are represented by continuous contours and shading. Negative zonal wind fields are represented by dotted contours. (c) Difference between surface winds (at 1000 hPa) simulated by CFS and observation (shown by wind vectors). JJAS mean zonal wind difference (m s^{-1}) between CFS and NCEP is represented by contours (negative values shown by dotted contours and positive values shown by continuous contours).

(BoB) experiences warm (cold) SST bias in general with decreasing (increasing) magnitude towards west (east) coast of India. The SST biases in CFS simulation over these two basins are quite important to explore, as they govern the performance of Indian monsoon rainfall to a great extent. In observations, both basins (AS and BoB) indicate bimodal distribution of SST. During monsoon season the SSTs are cooler as compared to they are in pre- and post-monsoon seasons. The cooler SSTs during monsoon may be due to mixing, evaporation and decrease of short-wave flux (pertaining to high cloud cover). Evaporation does not play a significant role during monsoon season in BoB due to large saturation as compared to AS (Lakshmi *et al*., 2009). Weaker south westerlies over AS in CFS as compared to that in NCEP may reduce mixing and evaporation and may lead to warm SST bias. The presence of relatively strong surface winds (at 1000 hPa) over western BoB (near east coast of India) in CFS (Figure 4) allows more mixing and in turn a deeper mixed layer (figure not shown) in the model, thus leading to a cold bias over this region.

4.1.3. Local SST–rainfall relationship

The convection over tropical Indian Ocean increases with warm SST, and the SST threshold of 27.5 °C initiates the organized deep convection (Gadgil *et al*., 2004). Other than SST threshold criterion, factors like large-scale convergence, SST gradient, etc., also play a significant role in determining the SST–rainfall relationship. Correlation between SST and rainfall field can provide information regarding oceanic impact on atmosphere. SST changes can be local and non-local. Non-local part depends on ocean advection and other dynamical factors of ocean. In this study, we shall focus on local changes of SST and the corresponding impact on rainfall. Local SST–rainfall relationship in CFS is investigated by examining the simultaneous correlation between rainfall and SST (Figure 5(a)). All correlations are computed on seasonal average (JJAS) of monthly anomalies after subtracting monthly climatological annual cycle. Correlations at 95% significant level are shown in Figure 5(a) and (b). For validation purpose, observed correlation

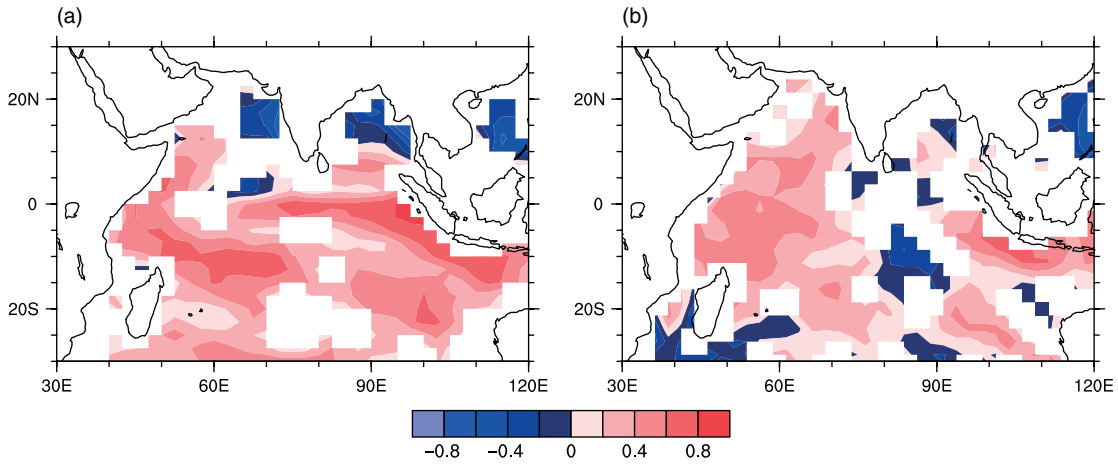

Figure 5. June–September (JJAS) average (data period: 30 years) pointwise and simultaneous correlations between precipitation and SST for (a) CFS (b) observation (Reynolds SST). Correlations at 95% significance level are shown.

between CMAP rainfall and Reynolds SST is also presented (Figure 5(b)). As the atmosphere responds rapidly to SST, a positive simultaneous correlation of rainfall and SST indicates SST's influence on the atmosphere (Bollasina and Nigam, 2009). This can be explained as follows: because of SST increase evaporation is likely to increase, which may lead to an increase in convection; consequently, it could result in more precipitation.

The precipitation–SST relationship is weak over a large part of Indian Ocean. However, it shows moderately large positive correlation over EIO near Indonesian region (Figure 5(b)). CFS also depicts moderately strong positive correlation near EIO region, although value of correlation is higher than that of the observation (Figure 5(a)). This shows the strong impact of ocean on the atmosphere in this region. WIO region also shows a positive correlation between rainfall and SST. CFS is able to capture it, although values are overestimated. The observation depicts a weak negative correlation over the central equatorial Indian Ocean (Figure 5(b)). On the other hand, CFS is not able to capture this negative correlation over the central equatorial Indian Ocean (Figure 5(a)). CFS-simulated SST–rainfall relationship is too strong in the equatorial Indian Ocean region. This is consistent with results of Bollasina and Nigam (2009). They have also noted that precipitation–SST link is too strong for IPCC (Intergovernmental Panel on Climate Change) – AR4-coupled simulation (twentieth-century climate integrations) of CCSM3 (Community Climate System Model), HadCM3 (Hadley Centre Coupled Model) and MIROC (Model for Interdisciplinary Research on Climate). They have also shown that SST control on local precipitation is weak in the observation. On the other hand, coupled models overestimate SST–rainfall relationship [e.g. the study by Wu *et al.*, 2006 for COLA (Center for Ocean-Land-Atmosphere Studies)-coupled model].

Over the warm region of BoB, the observed summer rainfall anomalies are negatively correlated with local SST anomalies (Rajeevan and Nanjundiah, 2009). AGCMs are unable to depict this negative relationship (Wang *et al.*, 2004). They concluded by stating that this problem is attributed to the experimental design in which the atmosphere is forced to respond passively to the specified SSTs, while in nature the SSTs result in part from the atmospheric forcing. Coupled models, pertaining to their atmosphere–ocean interactions, are better in simulating the SST–rainfall relationship (Wang *et al.*, 2004). CFS is able to capture the observed SST–rainfall relationship over BoB (Figure 5(a) and (b)). Thus, CFS has some success in simulating the observed SST–rainfall relationship over BoB. These results show that considerable improvements are still needed for these coupled climate models for realistic representation of SST–rainfall relationship.

4.1.4. *Lower tropospheric circulation*

Conjoined with prevailing biases of the rainfall, surface winds are also transformed. Normally, the Indian subcontinent region is characterized by a strong low level south westerly jet known as *Findlater jet* (Findlater, 1969), which peaks at around Somali coast and AS region. Wind patterns at 850 hPa are presented in Figure 6(a) and (b). Over the equatorial Indian Ocean, westerlies are predominant (north of equator). CFS mimics the observational findings somewhat realistically but the strength of the wind magnitude is quite weak as compared to that of NCEP (Figure 6(a) and (b)). The realistic simulation of mean surface winds is associated with the reasonable representation of surface latent heat flux (e.g. Hendon, 2000; Inness and Slingo, 2003). Zonal winds at 1000 hPa for CFS and observation are presented in Figure 4(a) and (b). Zonal winds in the CFS simulation are similar to the observed, although there are differences in magnitude. Zonal wind difference between CFS and observation is presented in Figure 4(c), and wind bias (CFS–observation) is also presented (shown by wind vector) in Figure 4(c). Easterly bias appears over the eastern Indian Ocean, near Indonesia. It is consistent with studies made by Seo *et al.* (2007). The presence

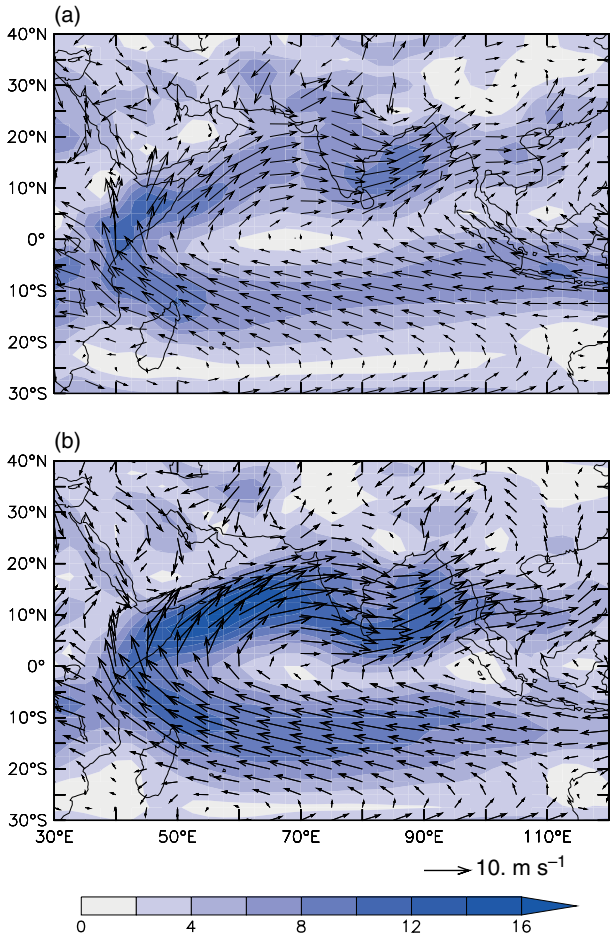

Figure 6. Wind climatology (m s^{-1}) at 850 hPa for (a) CFS and (b) NCEP reanalysis for JJAS. Shaded regions indicate wind speed.

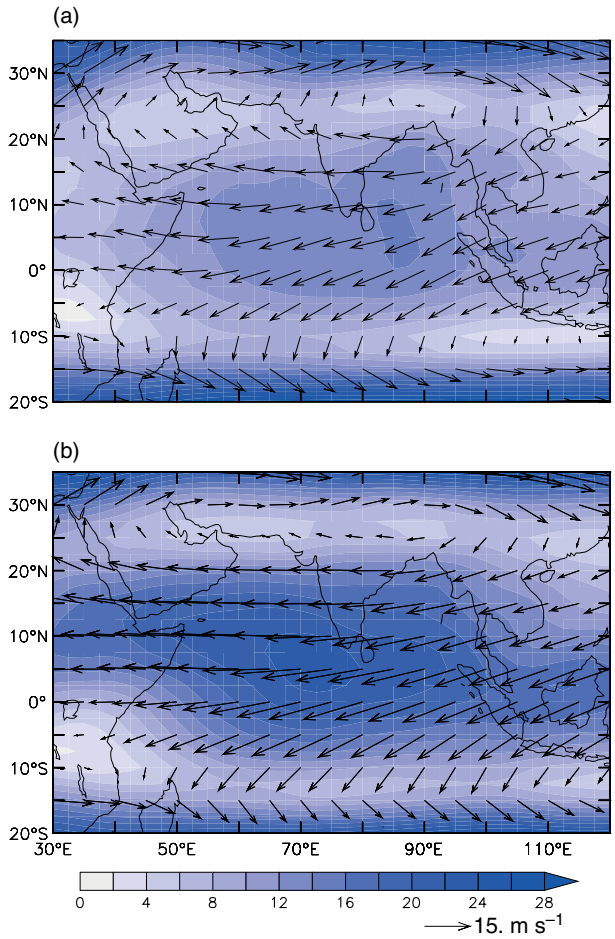

Figure 7. Wind climatology (m s^{-1}) at 200 hPa for (a) CFS and (b) NCEP reanalysis for JJAS. Shaded regions indicate wind speed.

of anomalous easterlies over Indian Ocean as compared to the observation is basically driven by the wet (dry) rainfall bias over west (east) Indian Ocean. Thus, these anomalous easterlies further drive the cold SST bias over the EIO by enhanced evaporation in CFS simulations. The evaporation bias of the model as compared to that of the observed latent heat flux (objectively analysed air–sea fluxes: OAFLUX) confirms the wet evaporation bias over EIO region (figure not shown). Thus, a coupled ocean–atmosphere feedback process starts and maintains the existing SST, rainfall and wind biases.

4.1.5. *Upper tropospheric circulation*

Upper tropospheric circulation at 200 hPa is characterized by the TEJ over the southern India and adjoining the equatorial Indian Ocean (Figure 7(b)). Strength of the easterly jet is an indication of monsoon activity over the Indian subcontinent (Naidu *et al*., 2011). CFS is able to simulate TEJ over the southern India and adjoining Indian Ocean, although it has lower magnitude as compared to the observation (Figure 7(a) and (b)). CFS is also able to simulate the position of the Tibetan High and its extensive ridge over the Asian region, which agrees with the observed climatology based on reanalysis (Figure 7(a) and (b)). The maximum strength of TEJ, as simulated on seasonal average basis, is 16 m s^{-1} in CFS. It is weaker than the observed strength of 22 m s^{-1}. In brief, CFS-simulated monsoon circulation is weaker than that of the observation. Weak monsoon circulation pattern may lead to less rainfall over the Indian subcontinent leading to dry rainfall bias over this region.

4.1.6. *Moisture convergence*

To get more dynamical insight, the divergent component of moisture transport and associated divergent wind vectors are presented in Figure 8(a) and (b). Moisture divergence takes place from the Mascarene high and moisture convergence takes place over India and at the head of BoB. Moisture divergence near Mascarene high region is weaker in the model as compared to that in the observation. Areal extent of moisture divergence is also smaller in CFS as compared to that in the observation (Figure 8(a) and (b)). In the model, the zero convergence anomaly line passes through central AS, whereas in the observation the line is closer to the west coast of India. For these reasons, convection near the west coast of India and part of AS is likely to be more in the CFS as compared to that in the observation.

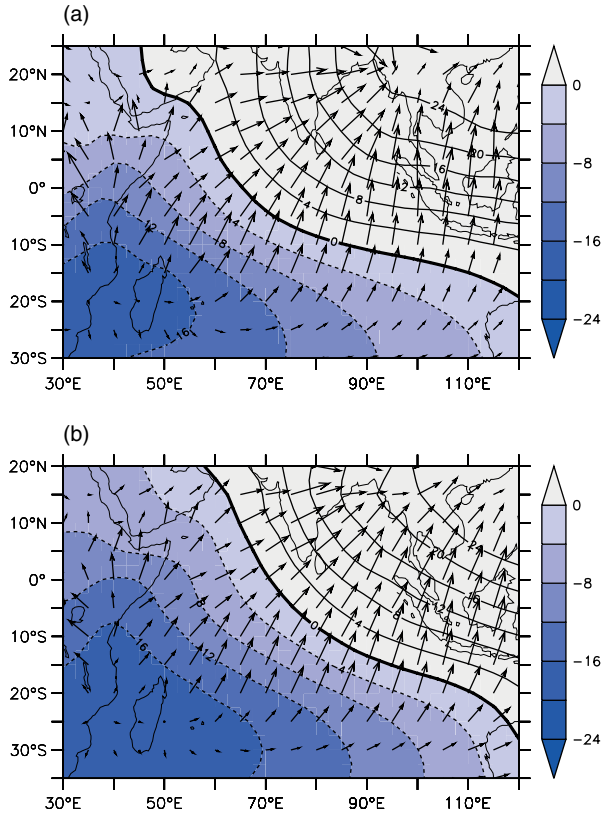

Figure 8. Divergent component of moisture transport [multiplied by 10^6 (kg s^{-1} m^{-1})] represented by shading/contours (negative values represented by dotted contours and positive values represented by continuous contours) and related moisture transport vectors for (a) CFS and (b) NCEP reanalysis.

The surface moisture convergence provides favorable condition for atmospheric instability which ultimately leads to convection. Therefore, wet biases of rainfall over parts of AS and western coast of India are noted (see Figure 1(c)).

4.1.7. Mean sea level pressure (MSLP)

Monsoon season is characterized by a steep surface pressure gradient between northern India and the southern Indian Ocean. This pressure gradient drives the wind from Southern Hemisphere to the monsoon region. It has been recognized in the earlier studies of Indian monsoon that the monsoon flows originate south of the equator (e.g. Blandford, 1874). The cross-equatorial flow (Somali jet) is an essential component of the Asian monsoon system (Findlater, 1969). It transports moisture from the southern Indian Ocean to the Indian region, and connects the Mascarene high and Indian monsoon trough.

The model-simulated and the observed NCEP reanalysis MSLP during monsoon (JJAS) is shown in Figure 9(a) and (b). One of the important features of the monsoon is the establishment of trough of low pressure over northern India. This monsoon trough is well simulated by the model (Figure 9(a)). The model also depicts high-pressure area over the southern Indian Ocean called *Mascarene high*. It is situated around 30 °S and 60 °E in NCEP

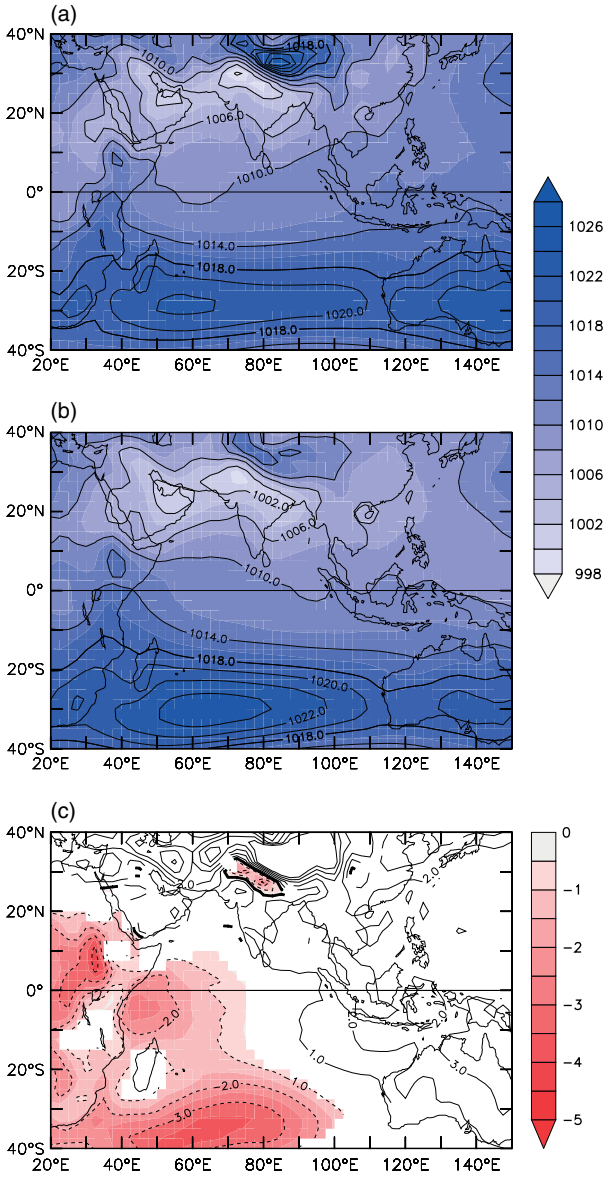

Figure 9. JJAS mean sea level pressure (hPa) for (a) CFS, (b) observation (NCEP reanalysis) and (c) difference between CFS and observation at 99% significant level (negative values are represented by dotted contours and shaded region and positive values are shown by continuous contours).

reanalysis data (Rao, 1976). CFS simulation indicates a slight shift of Mascarene high position by approximately 1° to the north (i.e. at 29 °S). MSLP model bias at 99% significant level is shown in Figure 9(c). CFS-simulated Mascarene high is underestimated as compared to that of the observation (Figure 9(a)–(c)). To examine the pressure gradient between northern India and Mascarene high, we define an index as the difference (B2–B1) in sea level pressure over region B2 (40 °S–15 °S, 30 °E–90 °E) and B1 (20 °N–30 °N, 70 °E–90 °E). This pressure gradient is 15 hPa in the model and 18 hPa in the observation. Over monsoon trough region (i.e. over box B1) the model-simulated pressure value is 1004 hPa and the observed pressure value is 1003 hPa. In brief, the model is able to simulate monsoon trough quite realistically.

In case of Mascarene high, the model-simulated value is 1019 hPa as compared to the observed climatological value of 1021 hPa. Pertaining to a weaker magnitude of Mascarene high, the model-simulated pressure gradient between northern India and the southern Indian Ocean is weak. Further to investigate reasons for the underestimation of high pressure over the southern Indian Ocean (Mascarene high), analysis of upper-level (200 hPa) SWJ stream is explored and possible physical mechanism is discussed in the following section.

4.2. Subtropical westerly jet (SWJ) and its role in model biases

SWJ is a high-speed meandering westerly wind current, aloft at the poleward edge of the Hadley cell over the subtropical areas as shown by a schematic (Figure 10). It is an integral part of the tropical Hadley circulation, which is mainly driven by thermal forcing. In the case of Southern Hemisphere SWJ, thermal forcing plays a major role, which itself is composed of SST distribution, latent heat release, continent–ocean heat contrast and heat flux convergence associated with transient eddies (Inatsu *et al*., 2000). The existence of strong north–south horizontal temperature gradient causes a westerly geostrophic wind pattern in the mid-latitudes because of Coriolis force. The thermal wind causes an increase in wind velocity with height, thus creating a strong SWJ stream (Holton, 1992). In this jet pure eastward motion cannot be sustained and the flow breaks down into large-scale eddies (turbulence) because of baroclinic instability. This baroclinic eddies break the Hadley circulation down, and stop the equatorial air from moving to the poles. However, in their circular motion, baroclinic eddies push warm air poleward and cold air southward, cooling the subtropics and warming the polar latitudes. This baroclinic eddies are the elemental part of the SWJ stream. The Northern and Southern Hemispheres exhibit similar jet stream patterns in the mid-latitudes. Thus, thermal wind criterion allows the strongest part of the jet stream should be in the proximity of the largest temperature gradients.

To explore the role of thermal forcing (i.e. SST distribution) in guiding the strength of SWJ, both SST and zonal wind at 200 hPa are plotted in the same panel (Figure 11). In the model simulations, warm SST region (represented by shaded region) is extended, over most parts of the globe, around the equator with the maximum over the Indian and Pacific basin and slightly reduced

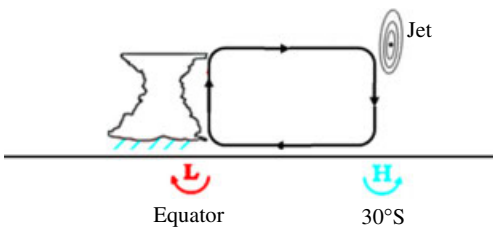

Figure 10. Schematic representation of Hadley cell circulation and upper-level subtropical westerly jet.

over the Atlantic basin (Figure 11(a)). However, in the observation the warmer SSTs are only over the warm-pool region of the eastern Pacific basin and some parts of Indian Ocean (Figure 11(b)). The Indian Ocean basin also has warm SST in the observation but not as intense and basin-wide as compared to the model. In the case of Atlantic basin, the SST values over 28 °C are completely missing in the observation. The observation shows that the zonally confined (35 °S–20 °S) SWJ core (represented by contours, zonal wind speed more than 34 m s^{-1}) is in line with SST distribution. It is also true for model simulations. In the case of the model, SWJ core is circum-global and the slightly reduced jet speed over Atlantic basin is also precisely concurring with the cooler SST region over the same meridian in the model. In the observation, SWJ core is located over Australia and the eastern Pacific basin precisely matching with warm SST regions located over the same meridian. These planetary-scale quasi-stationary waves are forced by large-scale zonally asymmetric heat source (Smagorinsky, 1953) and meridional temperature gradient. Figure 11(c) shows the meridional gradient of SST between equatorial region (10 °S–10°N) and subtropical area (35 °S–25 °S) along with the zonal wind at 200 hPa over subtropical area (35 °S–25 °S) for model and observation. The meridional (north–south) SST gradient (left axis) in the model (thin line, sstg mod) is always more than that in the observation (bold thick line, sstg obs), except at 80 °E–175 °E. This is the area of BoB, maritime continents and east Pacific warm-pool region, where SST gradient in the observation is more as compared to that in the model. This meridional SST gradient is reflected in terms of jet speed (right axis) quite accurately. Model jet speed (dotted line, u200 mod) is always more intense as compared to the observed jet speed (dashed line, u200 obs), except the areas where SST gradient of the observation is more than that in the model. Gaps in SST gradient curves represent land areas. In the observation, SWJ core is concentrated over Australian region by virtue of warm SST over Indonesian warm-pool region. In the model, the warm bias over tropical western Indian Ocean and eastern Pacific increases the meridional SST gradient over tropical Indo-Pacific Oceans. As a result, the model-simulated SWJ core is zonally elongated (circum-global) over Indo-pacific Oceans.

In the model, upper-level SWJ is circum-global and more intense as compared to that in the observation. This suggests that the model is simulating more mid-latitude disturbances in the Southern Hemisphere. The upper-level SWJ acts as a wave guide which intensifies the mid-latitude disturbances near the jet. The jets are refracted towards the core and extract energy from the mean flow (jet) for further development and propagation. The jet has the potential to enhance the geographical extent of low-frequency perturbations and tends to confine the disturbances to latitudes where the jet is centered. Since the disturbances are meridionally confined, their energy is not dispersed over a broad region and is able to propagate farther before being dissipated. The tendency for more

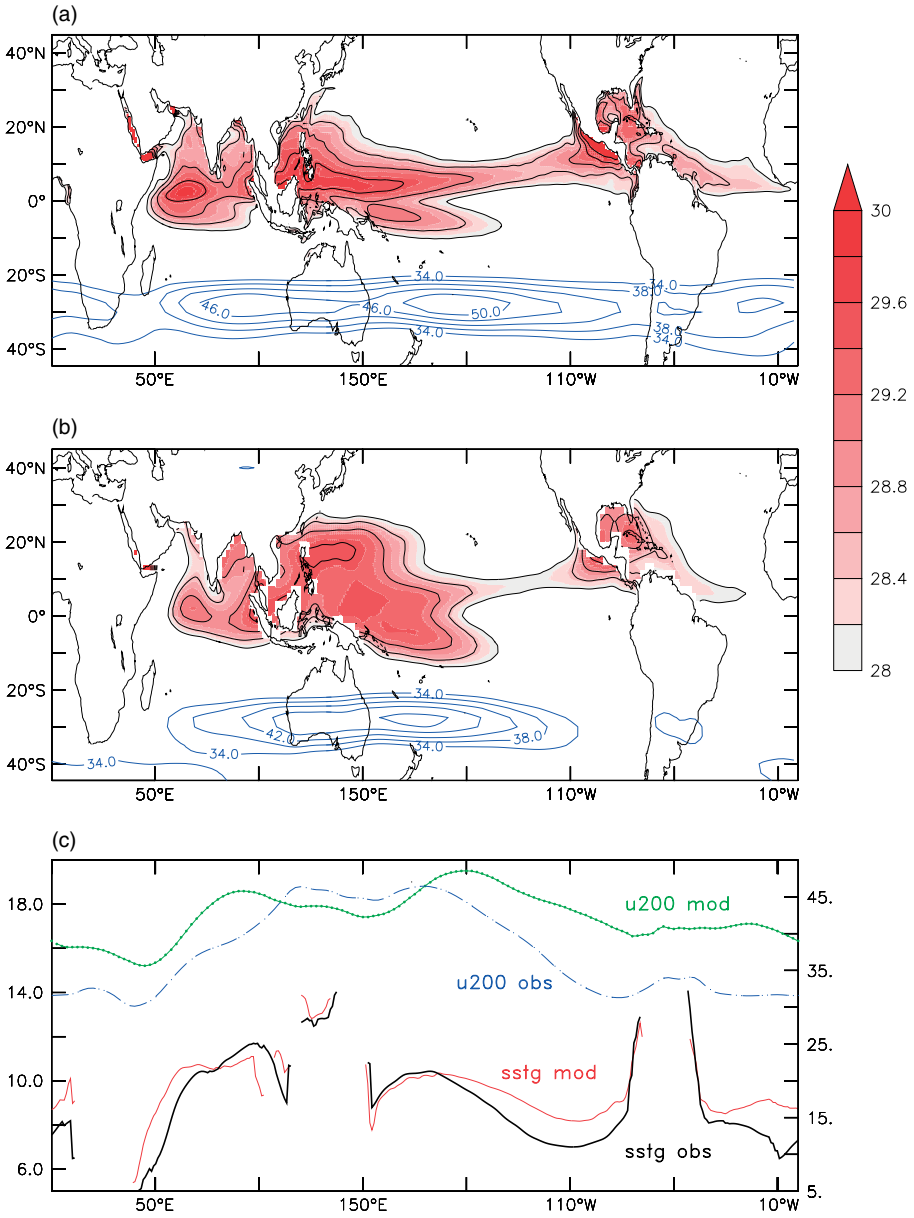

Figure 11. Distribution of SST (above 28 °C, represented by contours with shaded region) and zonal wind at 200 hPa (above 34 m s^{-1}, shown by contours) for (a) CFS and (b) observation. (c) Meridional gradient of SST (CFS: sstg mod represented by thin line; observation: sstg obs represented by bold thick line, shown on left axis) between equatorial region (10 °S–10°N) and subtropical area (35 °S–25 °S) along with the zonal wind at 200 hPa (CFS: u200 mod represented by dotted line; observation: u200 obs represented by dash line, shown on right axis) over subtropical area (averaged over region: 35 °S–25 °S).

extensive zonal energy propagation is further enhanced by the fact that the group velocity is proportional to the background winds, which are especially strong in the jet (Hoskins and Ambrizzi, 1993; Branstator, 2002). Further, the jet stream increases the upper-level horizontal shear as well as vertical shear throughout the troposphere. This leads to an increase in the barotropic and baroclinic instability over the region. The barotropic instability, which is associated with horizontal shear, grows by extracting kinetic energy from the jet stream. On the other hand, the baroclinic instability, which is associated with vertical shear, grows by converting the available potential energy associated with the mean horizontal temperature gradient, which provides thermal wind balance for the vertical shear in the jet stream. The upper-level horizontal shear increases the upper-level divergence towards its equatorward side of the jet stream core (Ramaswamy, 1956; Yadav *et al.*, 2009). The intensified disturbances increase troughs and low pressure areas, which reduces the surface pressure over the southern Indian Ocean (Mascarene high).

4.3. Feedback process for bias sustenance

The systematic bias of SST, rainfall and circulation present in the model sustains itself by coupled feedback processes. Each of the elements in this feedback loop either enhances or diminishes the effect of the corresponding element through the ocean–atmosphere coupled

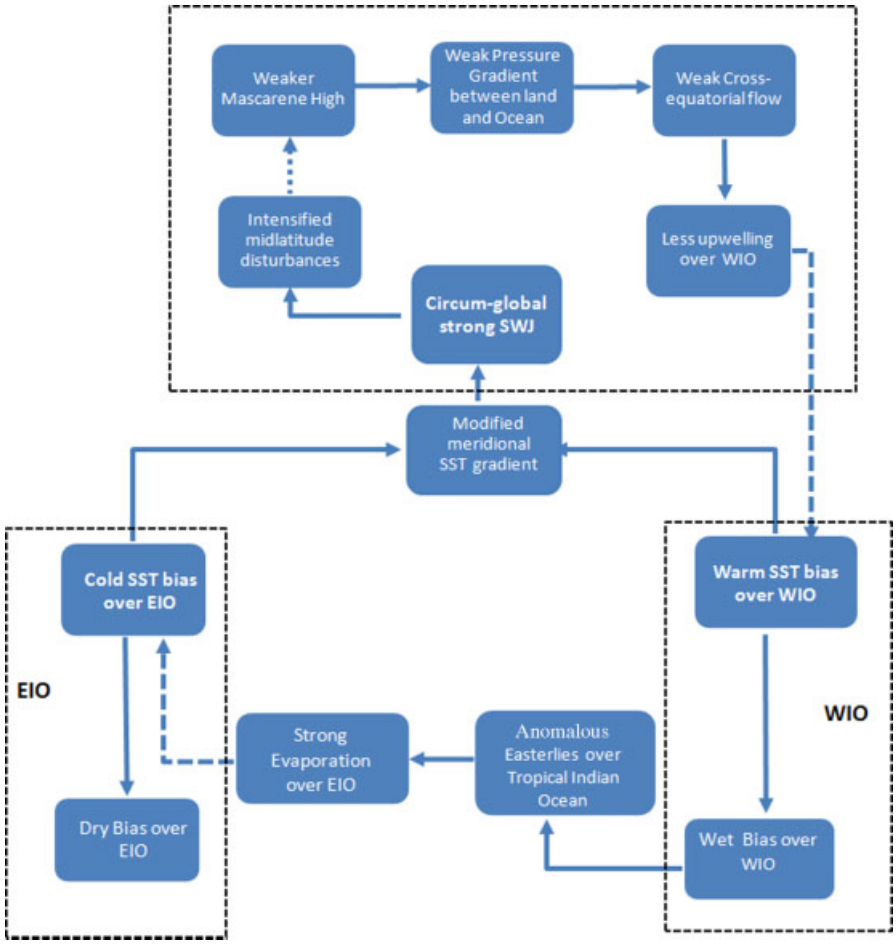

Figure 12. Schematic diagram illustrating coupled feedback process for bias sustenance. The positive (negative) feedback is shown by solid (dotted) arrow.

interactions. The exact cause and effect is very difficult to decipher but the interactions can be broadly summarized by a feedback loop as shown by the schematic diagram (Figure 12). Lower part of the proposed feedback loop is the extension of classical Bjerknes feedback. The presence of warm (cold) SST bias over west (east) Indian Ocean creates the zonal asymmetric heat source and modifies the meridional SST gradient. The subsistence of strong meridional SST gradient modifies the meridional Hadley circulation and strengthens the circum-global SWJ core (Inatsu *et al*., 2000), which in turn intensifies the mid-latitude disturbance and results in weaker Mascarene high. This persistence of weak Mascarene high reduces the very essential pressure gradient between land and ocean leading to a slower cross-equatorial flow. The weaker cross-equatorial flow in turn adds to less upwelling over Somalia coast and thus further driving the warm SST bias over WIO. Again the warm (cold) SST bias over west (east) Indian Ocean initiates the wet (dry) rainfall bias which again drives the easterly bias over tropical Indian Ocean. This easterly wind bias triggers evaporation and upwelling over EIO and advects warm waters towards WIO thus further driving the warm (cold) SST bias over west (east) Indian Ocean (Seo *et al*. 2007). The changes in SST over tropical Indian Ocean in response to changes in atmospheric variables (viz. rain, wind, etc.) and vice versa are a part of the classical Bjerknes feedback. However, how these biases in lower level connect to upper-level through the modulation of SWJ is the additional mechanism explored in this study. These systematic biases in the model simulation interact with each other and seem to enhance the error growth continuously through the feedback loop. However, it gets stabilizes as soon as the mean background state changes. Previous studies using SINTEX (Scale INTeraction EXperiment) model showed that intraseasonal oscillation of zonal winds excites equatorial downwelling Kelvin waves and deepens the thermocline in the eastern Indian Ocean, which in turn curtail the growth of SST bias over the eastern Indian Ocean (Rao and Yamagata, 2004; Rao *et al*., 2007). Apart from this, seasonal reversal of wind due to annual cycle of monsoon add to this and slowly model drift back to its own climatology. CFS also shows strong intraseasonal oscillation in rain and SST along with a strong annual cycle over the Indian Ocean region (Seo *et al*., 2007; Achuthavarier and Krishnamurthy, 2010b). Thus, similar feedback may occur in CFS also and consequently the system may stabilize.

5. Summary and conclusion

The seasonal mean monsoon climatology of the Indian region in long simulations of CFS is discussed in terms SST, rainfall and circulation biases. The feedback among SST, rainfall and circulation in lower level along with the interaction of upper-level SWJ in maintaining the model biases have also been explored. The model suffers from systematic warm (cold) SST bias over west (east) Indian Ocean and AS (BoB). The presence of significant SST bias between the model simulation and the observed climatologies is potentially associated with several processes governing the dynamics of the Indian Ocean basin. The region of these warm (cold) SST bias simultaneously co-occur with the region of wet (dry) rainfall bias, thus abiding by the local SST–rainfall relationship. This wet (dry) rainfall bias over west (east) Indian Ocean affects the circulation by inducing anomalous easterlies over tropical Indian Ocean. These easterly wind anomalies further drive the cold SST bias over EIO by triggering evaporation and warm SST bias over WIO by advecting warm waters. Thus bias sustenance of SST, rainfall and lower-level circulation in the model can be explained by atmosphere- and ocean-coupled feedback processes. These SST biases also magnify the upper-level circulation and in turn get intensified as well. Model SST bias maintains the meridional temperature gradient which in turn modifies the meridional Hadley circulation and transforms the upper-level SWJ. The presence of stronger meridional temperature gradient over the Indian Ocean region in the model establishes a zonally elongated SWJ core, which in turn magnifies the mid-latitude disturbances and decreases the Mascarene high as compared to that in the observation. The decreased Mascarene high weakens the pressure gradient between land and ocean and results in weak monsoon cross-equatorial flow as compared to that in the observation. The weakened cross-equatorial flow is associated with the less upwelling as compared to that in the observation, and thus further increasing the SST bias over the WIO. Thus SST, rainfall, and lower- and upper-level circulations mutually interact with each other through positive or negative feedback and cause the model biases over tropical Indian Ocean.

This type of study will help deciphering the model systematic errors and its associated coupled feedback mechanism to certain extent. Considering the complexity of dynamical and thermodynamical coupled physical processes involved in coupled models, determining reasons of model biases on the basis of a single study is a challenging task. Further studies need to be done for dealing with different components of the coupled system to explore more details about air–sea interaction processes.

Acknowledgements

Authors are thankful to Prof. B. N. Goswami, Director of IITM, for providing encouragement and support to carry out this work. The authors are thankful to COLA scientists, especially to Dr Jim Kinter, Prof. J. Shukla and Mr. Lary Marx for imparting training in CFS model. This research work was funded by SARAL AltiKa, SAC project on 'Ocean-Atmosphere Coupled Processes in Tropical Indian Ocean'. The authors are also thankful to NCEP group especially to Drs Arun Kumar, Suru Saha and S. Moorthi for the provision of GODAS initial condition data set required for running CFS. Critical comments by two anonymous reviewers are also acknowledged.

References

Achuthavarier D, Krishnamurthy V. 2010a. Daily modes of South Asian summer monsoon variability in the NCEP climate forecast system. *Climate Dynamics*. DOI: 10.1007/s00382-010-0844-9.

Achuthavarier D, Krishnamurthy V. 2010b. Relation between intraseasonal and interannual variability of the south Asian monsoon in the National Centers for Environmental Predictions forecast systems. *Journal of Geophysical Research* **115**: DOI:10.1029/2009JD012865.

Annamalai H, Xie SP, McCreary JP. 2005. Impact of Indian Ocean sea surface temperature on developing El Nino. *Journal of Climate* **18**: 302–319.

Behera SK, Krishnan R, Yamagata T. 1999. Unusual ocean atmosphere conditions in the tropical Indian Ocean during 1994. *Geophysical Research Letters* **26**: 3001–3004.

Blandford HF. 1874. The rainfall of northern India in relations to the temperature and the vapour constituents of the atmosphere. *Proc. Trans. Roy. Soc.* **164**: 563–653.

Bollasina M, Nigam S. 2009. Indian Ocean SST, evaporation, and precipitation during the South Asian summer monsoon in IPCC-AR4 coupled simulations. *Climate Dynamics* **33**: 1017–1032.

Branstator G. 2002. Circumglobal teleconnections, the jet stream waveguide, and the North Atlantic Oscillation. *Journal of Climate* **15**: 1893–1910.

Chen TC. 1985. Global water vapor flux and maintenance during FGGE. *Monthly Weather Review* **113**: 1801–1819.

Drbohlav L, Kyung H, Krishnamurthy V. 2010. Spatial structure, forecast errors, and predictability of the South Asian monsoon in CFS monthly retrospective forecasts. *Journal of Climate* **23**: 4750–4769.

Fennessy MJ, Kinter JL, Kirtman B, Marx L, Nigam S, Schneider E, Shukla J, Straus D, Vernekar A, Xul Y, Zhou J. 1994. The simulated Indian summer monsoon – a sensitivity study. *Journal of Climate* **7**: 33–43.

Findlater J. 1969. A major low-level air current near the Indian Ocean during the northern summer. *Quarterly Journal of the Royal Meteorological Society* **95**: 362–380.

Gadgil S, Sajani S. 1998. Monsoon precipitation in AMIP runs. *Climate Dynamics* **14**: 659–689.

Gadgil S, Vinaychandran PN, Francis PA. 2004. Extremes of Indian summer monsoon rainfall ENSO equatorial Indian Ocean Oscillation. *Geophysical Research Letters* **31**: DOI:10.1029/2004GL019733.

Gates WL, Boyle J, Covey C, Dease C, Doutriaux C, Drach R, Fiorino M, Gleckler P, Hnilo J, Marlais S, Phillips T, Potter G, Santer BD, Sperber KR, Taylor K, Williams D. 1999. An overview of the results of the Atmospheric Model Intercomparison Project (AMIP I). *Bulletin of the American Meteorological Society* **80**: 29–55.

Goswami BN. 1998. Inter-annual variations of Indian summer monsoon in a GCM: external conditions versus internal feedbacks. *Journal of Climate* **11**: 501–522.

Hack JJ, Keihl JT, Hurrell JW. 1998. The hydrologic and thermodynamic characteristic of the NCAR CCM3. *Journal Climate* **11**: 1179–1206.

Hendon HH. 2000. Impact of air-sea coupling on the Madden-Julian oscillation in a general circulation model. *Journal of Atmospheric Science* **57**: 3939–3952.

Holton JR. 1992. *An Introduction to Dynamic Meteorology*. Academic Press: San Diego, CA.

Hong S-Y, Pan H-L. 1998. Convective trigger function for a mass-flux cumulus parameterization scheme. *Monthly Weather Review* **126**: 2599–2620.

Hoskins BJ, Ambrizzi T. 1993. Rossby wave propagation on a realistic longitudinally varying flow. *Journal of Atmospheric Science* **50**: 1661–1671.

Hou Y-T, Campana KA, Yang S-K. 1996. Shortwave radiation calculations in the NCEP's global model. In *IRS'96: Current Problems of Atmospheric Radiation-Proceedings of the International Radiation Symposium*, Smith WL, Stamnes K (eds). A. Deepak Publishing: Fairbanks, AL, 317–319.

Inatsu M, Mukougawa H, Xie S-P. 2000. Formation of subtropical westerly jet core in an idealized GCM without mountains. *Geophysical Research Letters* **27**: 557–560.

Inness PM, Slingo JM. 2003. Simulation of the Madden-Julian oscillation in a coupled general circulation model, Part I: Comparisons with observations and an atmosphere-only GCM. *Journal of Climate* **16**: 345–364.

Kanamitsu M, Ebisuzaki W, Woollen J, Yang S-K, Hnilo JJ, Fiorino M, Potter GL. 2002. NCEP–DOE AMIP-II Reanalysis (R-2). *Bulletin of the American Meteorological Society* **83**: 1631–1643.

Kang I-S, Jin K, Wang B, Lau K-M, Shukla J, Krishnamurthy V, Schubert SD, Wailser DE, Stern WF, Kitoh A, Meehl GA, Kanamitsu M, Galin VY, Satyan V, Park C-K, Liu Y. 2002. Intercomparison of the climatological variations of Asian summer monsoon precipitation simulated by 10 GCMs. *Climate Dynamics* **19**: 383–395.

Kim YJ, Arakawa A. 1995. Improvement of orographic gravity wave parameterization using a mesoscale gravity wave model. *Journal of Atmospheric Sciences* **52**: 1875–1902.

Lakshmi V, Parekh A, Sarkar A. 2009. Bimodal variation of SST and related physical processes over the North Indian Ocean: special emphasis on satellite observations. *International Journal of Remote Sensing* **30**: 5865–5876.

Moorthi S, Pan HL, Caplan P. 2001. Changes to the 2001 NCEP operational MRF/AVN global analysis/forecast system. *NWS Technical Procedures Bulletin* **484**: 1–14. Available at www.nws.noaa.gov.

Naidu CV, Krishna KM, Rao SR, Kumar OSRUB, Durgalakshmi K, Ramakrishna SSVS. 2011. Variations of Indian summer monsoon rainfall induce the weakening of easterly jet stream in the warming environment?. *Global and Planetary Change* **33**: 1017–1032.

Pacanowski RC, Griffies SM. 1998. *MOM 3.0 Manual*. NOAA/ Geophysical Fluid Dynamics Laboratory: Princeton, NJ. Available at www.gfdl.noaa.gov.

Pattanaik DR, Kumar A. 2010. Prediction of summer monsoon rainfall over India using the NCEP climate forecast system. *Climate Dynamics* **34**: 557–572.

Rajeevan M, Nanjundiah RS. 2009. Coupled model simulations of twentieth century climate of the Indian summer monsoon. In *Current Trends in Science – Platinum Jubilee Special*, Mukunda N (ed). Indian Academy of Sciences: Bangalore. 537–567. Available at http://www.ias.ac.in/academy/pjubilee/book.html

Ramaswamy C. 1956. On the sub-tropical jet stream and its role in the development of large-scale convection. *Tellus* **8**: 26–60.

Rao YP. 1976. *Southwest Monsoon, Meteorological Monograph Synoptic Meteorology No. 1/1976*. India Meteorological Department: Pune.

Rao SA, Chaudhari HS, Pokhrel S, Goswami BN. 2010. Abnormal Indian summer monsoon of 2008: Role of southern Indian Ocean warming. *Journal of Climate* **23**: 5163–5174.

Rao SA, Masson S, Luo JJ, Behera SK, Yamagata T. 2007. Termination of Indian Ocean Dipole events in a coupled general circulation model. *Journal of Climate* **20**: 3018–3035.

Rao SA, Yamagata T. 2004. Abrupt termination of Indian Ocean Dipole events in response to intraseasonal disturbances. *Geophysical Research Letters* **31**: art no. L19306, DOI:10.1029/2004GL020842.

Reynolds RW, Rayner NA, Smith TM, Stokes DC, Wang W. 2002. An improved in situ and satellite SST analysis for climate. *Journal of Climate* **15**: 1609–1625.

Sabre M, Hodges K, Laval K, Polcher J, Désalmand F. 2000. Simulation of monsoon disturbances in the LMD GCM. *Monthly Weather Review* **128**: 3752–3771.

Saha S, Nadiga S, Thiaw C, Wang J, Wang W, Zhang Q, Van Den Dool HM, Pan H-L, Moorthi S, Behringer D, Stokes D, Pena M, Lord S, White G, Ebisuzaki W, Peng P, Xie P. 2006. The NCEP Climate Forecast System. *Journal of Climate* **19**: 3483–3517.

Seo K-H, Schemm J-KE, Wang W, Kumar A. 2007. The boreal summer intraseasonal oscillations simulated in the NCEP Climate Forecast System: The effect of Sea Surface Temperature. *Monthly Weather Review* **135**: 1807–1827.

Smagorinsky J. 1953. The dynamical influence of large-scale heat sources and sinks on the quasi-stationary mean motions of the atmosphere. *Quarterly Journal of the Royal Meteorological Society* **79**: 342–366.

Sperber KR, Brankovic C, Déqué M, Frederiksen CS, Graham R, Kitoh A, Kobayashi C, Palmer T, Puri K, Tennant W, Volodin E. 2001. Dynamical seasonal predictability of the Asian summer monsoon. *Monthly Weather Review* **129**: 2226–2248.

Sperber KR, Palmer TN. 1996. Inter-annual tropical rainfall variability in general circulation model simulations associated with the Atmospheric Model Inter-comparison Project. *Journal of Climate* **9**: 2727–2750.

Thiaw WM, Mo KC. 2005. Impact of sea surface temperature and soil moisture on seasonal rainfall prediction over the Sahel. *Journal of Climate* **18**: 5330–5343.

Wang B, Ding Q, Fu X, Kang I-S, Jin K, Shukla J, Doblas-Reyes F. 2005a. Fundamental challenge in simulation and prediction of summer monsoon rainfall. *Geophysical Research Letters* **32**: art no. L15711, DOI: 10.1029/2005GL022734.

Wang B, Kang I-S, Lee J-Y. 2004. Ensemble simulations of Asian-Australian monsoon variability by 11 AGCMs. *Journal of Climate* **17**: 803–818.

Wang W, Saha S, Pan H-L, Nadiga S, White G. 2005b. Simulation of ENSO in the new NCEP coupled forecast system model. *Monthly Weather Review* **133**: 1574–1593.

Webster PJ, Magana VO, Palmer TN, Shukla J, Tomas RA, Yanai M, Yasunari T. 1998. Monsoons: processes, predictability and the prospects for prediction. *Journal of Geophysical Research* **10**: 14451–14510.

Wu R, Kirtman BP. 2004. The tropospheric biennial oscillation of the monsoon-ENSO system in an interactive ensemble coupled GCM. *Journal of Climate* **17**: 1623–1640.

Wu R, Kirtman BP, Pegion K. 2006. Local air-sea relationship in observations and model simulations. *Journal of Climate* **19**: 4914–4932.

Wu X, Liang X, Zhang GJ. 2003. Seasonal migration of ITCZ precipitation across the equator: Why Can't GCMs simulate it. *Geophysical Research Letters* **30**: DOI:10.1029/2003GL017198.

Xie P, Arkin PA. 1997. Global precipitation: A 17 year monthly analysis based on gauge observation, satellite estimates and numerical model outputs. *Bulletin of the American Meteorological Society* **78**: 2539–2558.

Yadav RK, Rupa Kumar K, Rajeevan M. 2009. Increasing influence of ENSO and decreasing influence of AO/NAO in the recent decades over northwest India winter precipitation. *Journal of Geophysical Research* **114**: D12112, DOI:10.1029/2008JD011318.

Yang S, Zhang Z, Kousky VE, Higgins RW, Yoo S-H, Liang J, Fan Y. 2008. Simulations and seasonal prediction of the Asian summer monsoon in the NCEP climate forecast system. *Journal of Climate* **21**: 3755–3775.

Zhao QY, Carr FH. 1997. A prognostic cloud scheme for operational NWP models. *Monthly Weather Review* **125**: 1931–1953.

